Performance comparison of the spatial autocorrelation function and the mean intercept-length in the determination of trabecular bone anisotropy in the *in vivo* environment

M. J. Wald[1], B. Vasilic[1], P. K. Saha[1], F. W. Wehrli[1]

[1]Laboratory for Structural NMR Imaging, Department of Radiology, University of Pennsylvania Medical Center, Philadelphia, PA, United States

Introduction The degree of structural anisotropy of trabecular bone (TB) is of pivotal importance to its mechanical competence*(1)* and has been highly predictive of fracture risk in bone disease*(2)*. Micro-MR's non-invasive nature and high intrinsic bone-bone marrow contrast make it ideally suited for assessing TB microstructure in monitoring treatment and disease progression. Image processing techniques tailored to this application are needed to examine TB anisotropy. The mean-intercept-length (MIL) approach has been the primary user-independent method for quantifying fabric but its application to *in vivo* MRI has been limited. A faster method that relies on the spatial autocorrelation function and does not involve binarization has shown promise in measuring anisotropy of trabecular thickness (Tb.Th) and separation (Tb.Sp) *(3)*. In this work, the robustness of the ACF and MIL techniques are compared within the resolution and SNR limits of *in vivo* MR imaging.

Background and Theory: The spatial autocorrelation function computes the correlation distance (Tb.Th) and correlation wavelength (Tb.Sp) of a function (TB) based on the probability of finding two points (pixels) separated by a distance *n* and belonging to the same phase (bone or marrow). The ACF can be expressed as a spatial convolution (Eqn. 1) or as the inverse Fourier transform of the Fourier power spectral density (Eqn 2). Figures 1a-d, illustrate the principle of measuring the full-width at half-maximum (FWHM) and the correlation wavelength, d_1 of the ACF. These parameters estimate the mean Tb.Th and Tb.Sp along a given orientation. Some degree of periodicity is necessary for estimating of Tb.Sp. The speed of the Fourier transform is exploited to efficiently compute the ACF for multidimensional datasets. The mean intercept length is defined as the length of a test line across the object divided by the number of marrow or bone intercepts*(4)*. The principle is shown in Figure 1e for a μCT image with a voxel size of $(16\ \mu m)^3$. In a 3D dataset, by varying the polar (θ) and azimuthal (φ) angles, the MIL maps a second-rank tensor that characterizes the orientational dependence of a trabecular network*(5)*.

$$[1]\quad ACF[n] = \sum_{i=-\infty}^{\infty} f^*[i] \bullet f[n+i]$$

$$[2]\quad ACF[n] = \sum_{k=-\infty}^{\infty} |F[k]|^2 e^{jkn}$$

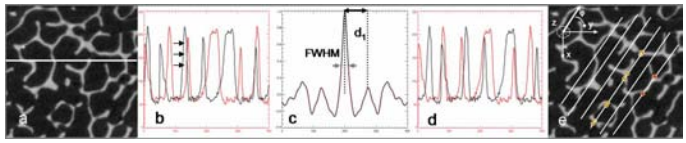

Figure 1. Test line through the image in (a) is plotted in (b) along with a shifted version of itself (black arrows). The ACF in (c) provides FWHM and d_1 metrics that estimate Tb.Th and Tb.Sp along test line. Original line and shifted version at d_1 in (d). Determination of MIL in (e) by the number of pixels belonging to bone/marrow divided by the number of traversals along profile.

Materials and Methods: The 3D ACF was sampled at angular increments of [θ, φ] so as to uniformly cover the sphere. In this manner FWHM and d_1 were determined along each angular direction. MIL was computed along the same angular directions, creating 3D ellipsoidal scatter plots for Tb.Th and Tb.Sp. The three eigenvectors of the covariance matrix for each measurement were computed by principal component analysis and their magnitudes were determined by a least-squares fitting procedure, resulting in ellipsoids representative of the fabric tensors. The ratio of the magnitudes of the smallest to the largest eigenvectors was computed as a measure of structural anisotropy. The programs (written in C and IDL) were designed to run on 3D μCT and μMR datasets of cadaveric bone and *in vivo* MR data obtained from a cubic volume of interest (VOI).

μCT images of the specimens from the distal radius at $(16\mu m)^3$ and *in vivo* MR datasets of the distal tibia acquired at $137x137x410\mu m^3$, subvoxel-processed to isotropic resolution $(69.5\mu m)^3$, were analyzed using both techniques. To evaluate the effect of noise characteristic of *in vivo* MR, complex noise was added to the spatial frequency domain of a μCT dataset which, upon inverse Fourier transformation, manifests as a Rician noise distribution in the magnitude image, shown in Figures 2a-d. Partial-volume blurring was simulated by low-pass filtering the spatial frequency data using Gaussian filters with varying standard deviations, σ. In this manner, images ranging in effective resolution from $16\text{-}100\mu m^3$ were created. The effects of RF coil shading were examined using VOIs from *in vivo* scans of the distal tibia from three subjects*(6)*. For each scan, the normalized coil sensitivity map, shown in Figure 3b, was estimated at each point within the cortical shell as the 20th percentile of the intensity histogram defined over a spherical volumetric neighborhood. A VOI was selected from each scan and analyzed using both MIL and ACF techniques with and without the contribution of the coil shading map (Figures 3a, 3c, and 4). The shading-free VOI was then subjected to the shading from four randomly chosen regions (Fig. 4b) and the variations of MIL and ACF with respect to location within the sensitivity profile were quantified as a percentage error (σ from all 5 regions of coil shading divided by the mean).

Figure 2. Top: Images ranging in CNR from 5.2 to 1.8. Bottom: Effects of noise on MIL and ACF anisotropies.

Figure 3. a) Slice of distal tibia scan from coil shading analysis, left-right corresponds to anterior-posterior b) Coil shading map with location of VOI and regions of shading used (dotted boxes). c) Magnified view of VOI.

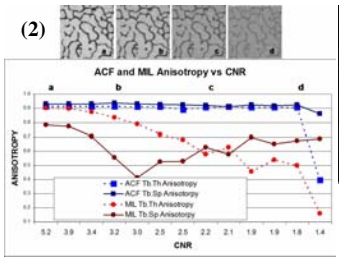

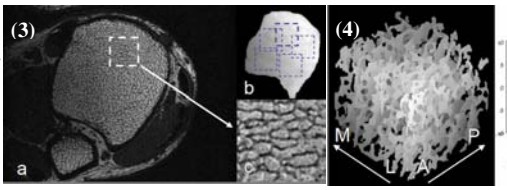

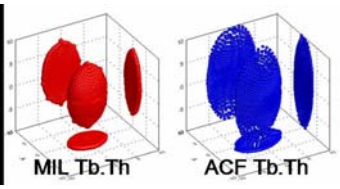

Figure 4. Cubic subvolume rendering from distal tibia of subject used in inhomogeneity analysis with Tb.Th ellipsoids from MIL(red) and ACF(blue). ACF ellipsoid is more anisotropic than MIL. Plot axes match image axes (Up is infero-superior direction) and projections indicate perspective views of the ellipsoids.

Results: The ACF computation was found to be ~150 times faster than the MIL for a 100x100x100 byte dataset. Figure 2 shows images at four different contrast-to-noise ratios (CNRs) and the dependence of both the Tb.Th and Tb.Sp anisotropies measured by ACF and MIL. ACF measures of anisotropy were found to be insensitive to noise levels down to CNR of ~1.8. Tb.Sp anisotropy of MIL and ACF were plotted with respect to the standard deviation of the low-pass Gaussian apodization filter (not shown). The ACF measurement demonstrated relative insensitivity to resolution degradation, while the MIL–derived values increased significantly (approximately 5 times more dependent than ACF) with an increase in the number of partially-volumed voxels. The Tb.Th anisotropies of the two techniques were equally robust under low-pass filtering. With respect to RF coil shading, the ACF was found do be more robust than MIL from repeated measurements under the influence of different regions of coil shading. The largest disparity in percentage errors was in the magnitudes of the longitudinal component of the Tb.Th and Tb.Sp tensors, which for the ACF were 1.4% and 6.6% versus 8.5% and 9.7% for MIL, respectively. Fig. 4 shows the $(7mm)^3$ VOI outlined in Figures 3a and 3c from an *in vivo* scan of a distal tibia used in the coil shading analysis. The resulting ellipsoids in Figure 4 were calculated using MIL and ACF and indicate the orientational dependence of Tb.Th within the VOI. Both ellipsoids are smooth and specify the longitudinal, infero-superior direction as the direction of the largest and the antero-posterior direction as the second-largest eigenvalues, as expected. The ratio of the shortest to the longest tensor components were 0.378 for MIL and 0.314 for ACF.

Conclusions: The ACF derived parameters are less sensitive to noise, RF coil shading, and partial voluming than MIL. Further, ACF-derived measurements of Tb.Th, Tb.Sp, and anisotropy do not require binarization of the images and therefore are particularly suited for the analysis of *in vivo* images. Lastly, the computation is significantly faster than for MIL since it can be computed in the spatial frequency domain.

References: (*1) S. C. Cowin, J Biomech. Eng.* ***108****, 83 (1986). (2) T. E. Ciarelli et al., JBMR* ***15****, 32 (2000). (3) M. J. Wald et al., SPIE Med. Imag.* ***5746*** *291 (2005). (4) W. J. Whitehouse, J Microsc.* ***101*** *Pt 2, 153 (1974). (5) M. R. Harrigan, J. Mat. Sci.* ***19****, 761 (1984). (6) B. R. Gomberg et al., Bone* ***35****, 266-76 (Jul, 2004).*

Acknowledgements: NIH R01 AR 41443, NIH R01 AR 49553, NIH T32-EB000814